npj Science of Food

https://doi.org/10.1038/s41538-026-00814-7

Article in Press

The regulation mechanism of α-linolenic acid bioavailability by flaxseed lignan macromolecules in O/W emulsions

Received: 8 August 2025

Accepted: 16 March 2026

Cite this article as: Cheng, C., Yu, X., Wang, L. *et al.* The regulation mechanism of α-linolenic acid bioavailability by flaxseed lignan macromolecules in O/W emulsions. *npj Sci Food* (2026). https://doi.org/10.1038/s41538-026-00814-7

Chen Cheng, Xiao Yu, Lei Wang, Shuyi Li, Xu Chen, Qianchun Deng & Zhenzhou Zhu

The Regulation Mechanism of α-Linolenic Acid Bioavailability by Flaxseed Lignan Macromolecules in O/W emulsions

Chen Cheng[a], Xiao Yu[b,c], Lei Wang[b], Shuyi Li[a], Xu Chen[a*], Qianchun Deng[b*], Zhenzhou Zhu[a]

a. National R&D Center for Se-rich Agricultural Products Processing, Hubei Engineering Research Center for Deep Processing of Green Se-rich Agricultural Products, School of Modern Industry for Selenium Science and Engineering, Wuhan Polytechnic University, Wuhan 430023, China

b. Oil Crops Research Institute of the Chinese Academy of Agricultural Sciences, Hubei Key Laboratory of Lipid Chemistry and Nutrition, and Key Laboratory of Oilseeds Processing, Oil crops and Lipids Process Technology National & Local Joint Engineering Laboratory, Wuhan 430062, China

c. College of Food and Bioengineering, Henan Key Laboratory of Cold Chain Food Quality and Safety Control, Zhengzhou University of Light Industry, Zhengzhou 450001, China

*Corresponding author: Prof. Xu Chen (chxu@whpu.edu.cn); Prof. Qianchun Deng (dengqianchun@caas.cn)

Abstract

Enhanced α-linolenic acid (ALA) intake effectively alleviates population sub-health status through dietary pattern modification, demonstrating substantial implications for promoting national health advancement. In this study, the multi-targeted regulation on ALA micellization, absorption, and lymphatic transport by natural flaxseed lignan macromolecules (FLM) and its thermal treatment products (FLM 150) was systematically investigated in emulsion delivery system. *In vitro* Caco-2 transport assays revealed that ALA absorption was enhanced by 95% with the addition of FLM 150. Moreover, in vivo rat mesenteric lymph cannulation proved that FLM 150-enriched emulsion elevated ALA absorption by 493%, while significantly reduced lipid oxidation. Besides, lipidomic profiling indicated that FLM 150 enhanced triglyceride resynthesis during lipid resynthesis in intestinal epithelial cell, as well as promoted metabolism of ALA. Therefore, these findings established FLM 150 as a multi-target regulator optimizing ALA bioavailability through concurrent mucosal barrier reinforcement, oxidative stress mitigation, and lipid metabolic pathway redirection. And these insights highlighted the potential of engineered emulsion systems to lipid absorption kinetics and intestinal metabolic outcomes, offering novel strategies for enhancing the bioavailability of ALA.

Keywords: Flaxseed Lignan Macromolecules, α-linolenic acid, Emulsion, Lipid oxidation, Bioavailability

1. Introduction

The rapid economic development of recent decades has precipitated profound shifts characterized by decreased physical activity and ultra-processed food consumption, contributing to a global health crisis marked by widespread metabolic imbalance. According to the epidemiological investigation by World Health Organization, over 75% of the global population now suffers from suboptimal health conditions due to obesity, with the Insufficient intake of polyunsaturated fatty acids (PUFAs) emerging as a key contributing factor. α-linolenic acid (ALA), a plant-derived n-3 PUFAs, was also reported to play a pivotal role in modulating immune function, reducing cardiovascular risks[1]. Research indicated that enhancing ALA intake through dietary restructuring thus represents a critical strategy to address public health challenges and improve population-wide well-being, especially for child and adolescent obesity[2]. However, the high degree of unsaturation in ALA confers significant susceptibility to oxidation, with both in vitro studies and in vivo models demonstrating accelerated oxidative degradation. This process generates free radicals and promotes lipid peroxidation, thereby significantly compromising ALA's bioavailability, reducing its biological activity, and potentially inducing oxidative stress-related tissue damage.

Upon oral ingestion, FO is sequentially processed, starting with gastrointestinal pre-emulsification, progressing to lipolysis and intestinal release of products, followed by epithelial uptake, and ultimately reaching systemic circulation to exert its bioactivities[3]. Besides, the intestinal absorption of free fatty acids (FFAs) etc. lipolysis products involve multiple critical steps that continue to influence the subsequent metabolic fate of ALA *in vivo*. Those processes include the mixed micelle formation, mucus layer penetration, transmembrane transport into enterocytes, and re-esterification of triglycerides (TG), and chylomicrons (CMs) assembly[4]. Mucus layer penetration is the key step to absorption of nutrients, which has received a lot of attention recently[5]. The mucus layer, a biological gel-like network with a thickness of approximately 50-200 μm lining the gastrointestinal tract, serves as a selective barrier that restricts passage of toxic compounds, pathogenic bacteria, and viruses while permitting nutrient absorption

by intestinal epithelial cells[6]. Current evidence suggested that small hydrophilic molecules generally diffused freely through this protective layer, whereas larger exogenous substances frequently experienced entrapment due to steric hindrance effects or interactions mediated through electrostatic forces, hydrophobic associations, and hydrogen bonding with mucus components[7]. Therefore, the diffusion behavior of the mixed micelles in the mucus layer and the transmembrane process of small intestinal epithelial cells are of great significance for the efficient absorption of ALA[8]. This mechanistic framework underscores the biological significance of two sequential processes: 1) the diffusive transport of mixed micelles through the mucus barrier, and 2) the subsequent transmembrane uptake by enterocytes. Both stages collectively govern the overall absorption efficiency of ALA, thereby influencing its downstream metabolic utilization as well as bioavailability.

Reports indicated that emerging emulsion engineering strategies demonstrated the high-efficiency delivery of PUFAs through micellar solubilization enhancement and lymphatic transport optimization. For instance, phospholipid-stabilized flaxseed oil (FO) emulsions leveraged interfacial engineering to enhance lipid stability, digestion kinetics, and absorption efficiency[9]. Pharmacokinetic analyses revealed that nanostructured emulsions accelerated lipase-mediated triacylglycerol hydrolysis and micellar solubilization, which further elevated ALA bioavailability by 129%[10]. Therefore, constructing an emulsion delivery system using phospholipids as an emulsifier is a promising strategy to enhance the bioavailability of ALA. Notwithstanding these advancements, a persistent challenge arises when using plants phospholipids to formulate ALA-enriched emulsions: the "core-membrane co-oxidation" phenomenon caused by the PUFA chains both in ALA and phospholipids[11]. The simultaneous oxidation of lipid cores and interfacial layers accelerates ALA degradation, compromising colloidal stability. This oxidative vulnerability highlights an urgent need to identify compatible antioxidants capable of preserving ALA integrity in phospholipids-based emulsion systems without compromising their digestive or absorptive advantages[12]. Addressing this gap, it needs to focus on developing oxidation-resistant, functionally optimized ALA delivery systems by integrating novel antioxidant strategies with interfacial

engineering.

For nano-scale nutrient carriers such as ALA-containing mixed micelles, the rheological properties of the mucus layer, particularly its viscosity, play a pivotal role in determining permeation efficiency, with emerging research indicating significant modulation of these parameters by dietary polyphenols[13]. Flaxseed lignans, a class of lipid concomitants in FO, exhibited multifaceted physiological functions including prevention of ovarian cancer, cardiovascular diseases, oxidative stress, and inflammatory responses[14-15]. Lignans exist as secoisolariciresinol diglucoside (SDG) oligomers in their native state, collectively termed flaxseed lignan macromolecules (FLM). Emerging evidence highlighted SDG's functionality in stabilizing whey protein/phospholipid-based FO emulsions during storage while simultaneously enhancing ALA release kinetics during intestinal digestion[9]. Mechanistic investigations revealed that SDG potentiated intestinal absorption of FFAs from emulsion systems through multiple pathways: stimulation of bile secretion, amplification of micelle generation, upregulation of apolipoprotein expression, as well as facilitation of chylomicron assembly[16]. These properties established SDG as a unique polyphenolic compound, which had capable of concurrently mitigating ALA oxidation and improving its bioavailability. Intriguingly, FLM demonstrated pharmacokinetic and bio-functional equivalence to its structural subunit SDG, positioning it can be a cost-effective and sustainable alternative for large-scale applications[17-18].

Our previous findings indicated that both FLM and its thermally processed derivatives under 150°C (FLM 150) modulated intestinal digestion kinetics in sunflower phospholipid-stabilized ALA-rich emulsions[19-20]. Specifically, FLM exerted antioxidant activity and digestive enzyme inhibition, thereby retarding FFA liberation during small intestinal digestion[20]. Notably, FLM 150 induced structural modifications of FLM that enhanced FFAs release efficiency from FO emulsion. Our previous research efforts elucidated that the structural plasticity of FLM, coupled with its demonstrated bioactivity and antioxidative activity, positions it as a promising functional ingredient for nutraceutical and pharmaceutical formulations requiring precise control over lipid digestion kinetics. Based on above research, the mechanistic interplay between flaxseed lignan

derivatives and ALA absorption is an urgent need for in-depth research. Therefore, the current experiment integrates *ex vivo* mucus barrier models to quantify micelle-mucus interactions and delineate the physicochemical determinants of barrier penetration. Complementary *in vitro* and *in vivo* absorption models were implemented, including Caco-2 intestinal epithelium monolayers for transmembrane transport assessment and mesenteric lymph duct cannulation in rats for chylomicron-mediated lipid transport analysis. Through this comprehensive experimental strategy, the study aims to establish structure-function relationships governing lignan-enhanced ALA bioavailability, providing critical insights for designing functional emulsion systems with optimized nutraceutical delivery profiles.

2. Results and discussion

2.1 In vitro evaluation the effect of different flaxseed lignans on the absorption of ALA

In general, the gastrointestinal (GI) tract is covered by mucus, which comprises a firmly adhered, nonstirred viscous inner layer tightly attaching to the epithelium, and a loosely adherent, less viscous outer layer remote from the epithelium [21]. Therefore, the released free fatty acids from FO emulsions after intestinal digestion need to be successfully permeated through mucus, that can be further absorbed by intestinal epithelial cells[22]. In our study, the reconstituted mucus model was established to simulate the permeation of ALA enriched micelles through mucus layer. As shown in Figure 1a, to establish a visualization model for mucus layer permeability, the mucus was extracted and purified from the mucosa and then labeled with Fluor 488-labeled wheat germ agglutinin (WGA)[13]. Prior to the permeability experiment, BODIBY 488-C12 was used to label the mixed micelles, and the process of mixed micelles through reconstituted mucus was recorded using the Z-scans of a wide area of Leica Confocal Laser Scanning Microscope (CLSM, Germany).

As Z-stack 3D images and its corresponding cross-sectional views shown in Figure 1b and c, at the initial stage of permeation (0 min), BODIBY 488-C12-labeled mixed micelles (red fluorescence) were localized on the surface of the mucus layer. The results of cross-sectional images of the top (0 μm) and middle layers (10 μm) of the mucus layer revealed no red fluorescence in the middle layer at 0 min, indicating that labeled micelles confined on the top of mucus layer.

After 10 minutes of permeation, the cross-sectional images for the middle (10 μm) and bottom layers (20 μm) had the red fluorescence in Control and FLM groups, while the FLM 150 group showed no fluorescence in the bottom layer. These results indicated that mixed micelles in the Control and FLM groups fully penetrated the 20 μm mucus layer within 10 minutes, while FLM 150 exhibited the limited permeability (<20 μm). The static rheological test of the mucus layer proved that FLM 150 significantly increased the apparent viscosity of the mucus layer, thereby reducing the penetration of micelles in the mucus layer[13].

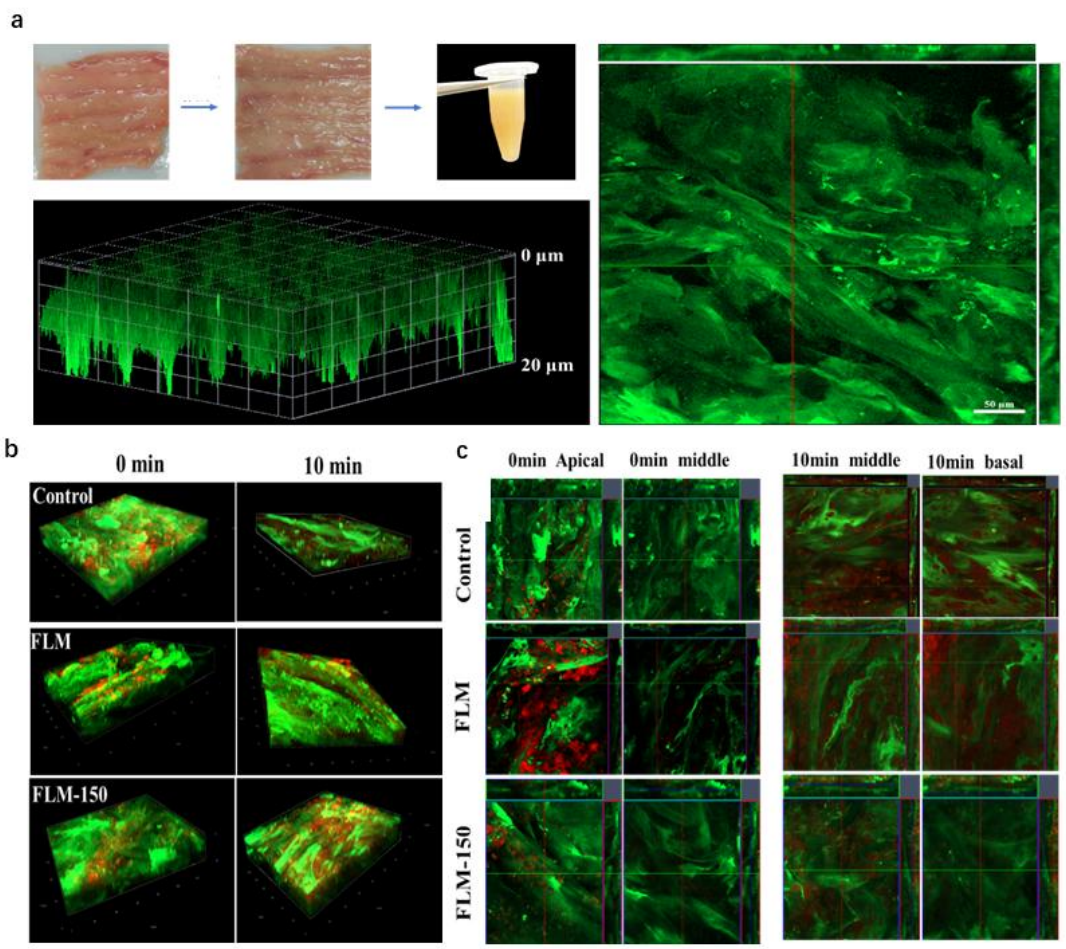

Fig. 1

(a)Morphology and micromorphology (labeled using Alexa Fluor-conjugated WGA) of the mucus layer *ex vivo*; (b) Confocal images of the Z-scans of a wide area of mucus layer show the penetration of ALA micelles (labeled with BODIBY 488-C12 in red) into the reconstituted mucus layer; (c) Two-dimensional coverage of different ALA micelles labeled with BODIBY 488-C12 (red) diffusing in the intestinal mucus labeled with Alexa Fluor 488-WGA (green) ex vivo. Depth: 0−20 μm after 10min penetration.

The transport and absorption process of ALA was simulated using Caco-2 cells model. The cytotoxicity of the tested mixed micelles in differentiated Caco-2 cells was determined by MTT method. As shown in Supplement table 1, after treatment with the 100-fold diluted micelle solution, Caco-2 cells viability remained more than 2/3, indicating that the 100-fold diluted micelles can be used for the next cell absorption experiment. The quantitative result of ALA in the basal of *Transwell* was monitored to evaluate its absorption kinetics (Fig.2). During the first 30 minutes of absorption, approximately 2.8 μg of ALA underwent transcellular transport from the apical to the basolateral side through Caco-2 cell monolayers in both the control and SDG groups, with no significant difference ($p<0.05$) observed between the groups. About 1.3 - 1.5 μg of ALA was transcellular transported in SECO, FLM, and FLM 150 groups. About 0.57 μg of ALA was transcellular transported in emulsifier S90 group. After 120 minutes of absorption, transcellular transport of ALA peaked in the FLM 150 and SDG groups at approximately 9.5 μg. Compared to the Control, both FLM 150 and SDG significantly enhanced ALA absorption within the emulsion system, achieving a 95% increase. Furthermore, FLM-supplemented and SECO-supplemented FO emulsions increased ALA absorption by 32.5% and 14.2%, respectively, relative to the Control.

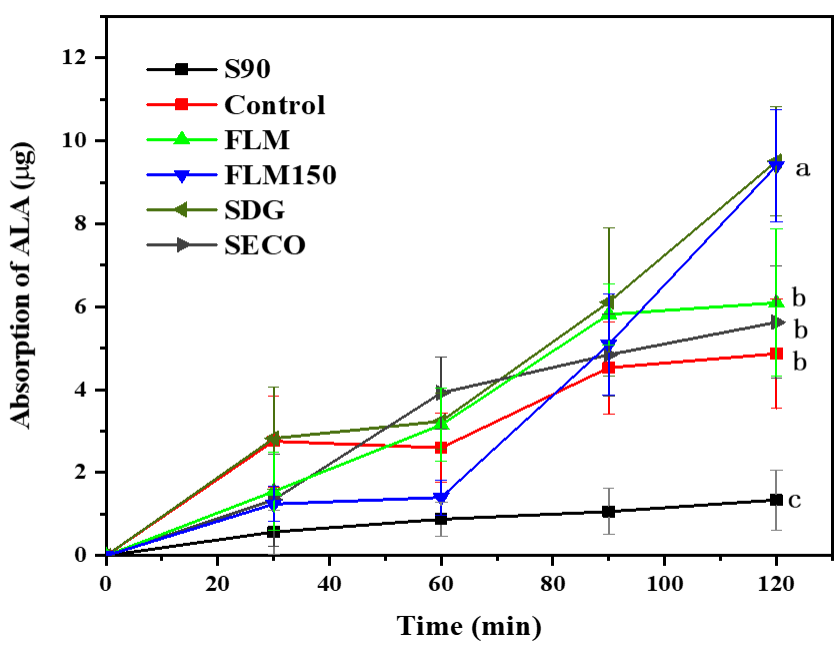

Fig.2 the absorption kinetic of ALA by Caco-2 small intestinal epithelial cells model. (Different letters indicate

statistically significant differences at $p<0.05$, FLM 150 and SDG had no significant difference)

During absorption experiments, baseline ALA was measured in the basolateral chamber of *Transwell* systems for the S90 group (sunflower phospholipid without FO supplementation). This background detection stems from ALA being a native component of sunflower seed phospholipids[11]. Compared to the Control and SDG-supplemented groups, FO emulsions containing weak-polar flaxseed lignans (SECO, FLM, FLM 150) exhibited significantly reduced early-phase ALA absorption kinetics (first 30 min; $p < 0.05$). FLM 150 supplementation resulted in the lowest ALA absorption rate among all groups, as weak-polar lignan-mucus self-association reduced ALA penetrability through the mucus layer and absorption into intestinal epithelial cells[13, 23].

2.2 In vivo verification the effect of different flaxseed lignans on the absorption of ALA

Following digestion of FO in the intestine, the absorbed ALA are re-esterified into triglycerides within the enterocytes and packaged into chylomicrons. These chylomicrons are then exclusively secreted into the intestinal lymphatic system. Therefore, lymph is the first and most direct bodily fluid to carry the newly absorbed ALA before it enters the general circulation and undergoes metabolism in the liver and peripheral tissues[3]. In our study, a mesenteric lymph duct cannulation experiment was conducted in rats to further evaluate the impact of FLM and FLM150 on ALA absorption. As illustrated in Figure 3A, CMs in the lymph fluid collected from all samples exhibited uniformly spherical and structurally regular morphologies across all time intervals. Figure 3B further delineated the CMs particle size. Prior to gavage, the baseline particle sizes of CMs in all groups showed no significant differences, averaging approximately 150 nm. After oral FO administration alone, the mean CMs diameter in lymph fluid increased to 262.4 nm within 0–1 h, reached a peak of 520.18 nm at 1–2 h, and subsequently fell gradually to 202.37 nm by 8–24 h. In comparison, the Control group (FO emulsion gavage) displayed a similar trend, with CMs size reaching a maximum of 512.91 nm at 1–2 h, maintaining this peak until 2–4 h, and then gradually decreasing to 204.96 nm by 12–24 h. These findings indicate that FO nanoemulsification increased CMs' particle size during lymphatic synthesis, enhancing lipid transport efficiency. This effect likely stems from co-ingested sunflower phospholipid, which supply additional structural

components for CM assembly[24]. The observation of sustained larger CM size in the Control group compared to FO during the 2–4 h interval implies a prolongation of lipid absorption by nanoemulsification. Under the present experimental conditions, neither FLM nor its lignan derivatives (SDG/SECO) affected the structural integrity of CMs, as comparative analysis showed no significant morphological differences among the Control, gavage FLM, FLM 150, SDG-enriched, or SECO-enriched emulsion groups.

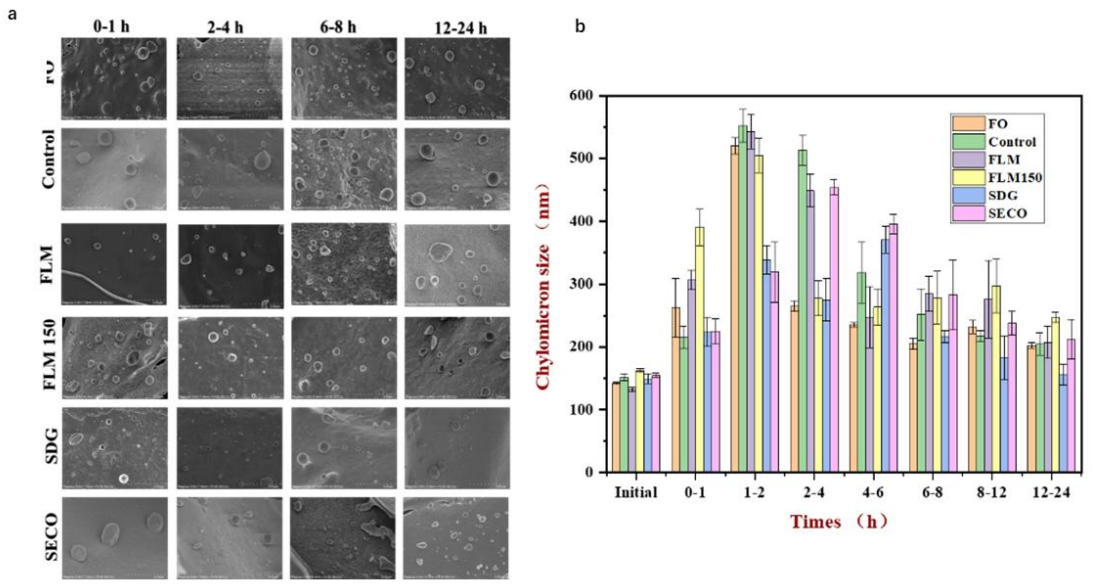

Fig.3 Effect of FLM, FLM150-enriched emulsion on lymphatic CMs' microstructure (a) and particle size distribution (b) after gavage.

These results collectively highlighted the critical role of co-nanoemulsification of ALA and different flaxseed lignans in modulating lymphatic lipid transport kinetics. In comparison to Control (FO emulsion group garage), rats administered FLM enriched FO emulsions (FLM) exhibited a maximum CMs' particle size in lymph at 1-2 h, which decreased to 207.6 nm during 2-12 h and further reduced to 247.6 nm at 12-24 h. However, the FLM 150 group (FLM 150 enriched FO emulsions gavage) demonstrated a significantly larger peak CMs' size of 504.7 nm at 1-2 h. Notably, the FLM 150 group showed 48.8% higher CMs' particle sizes ($P<0.05$) than the FO group during 0-1 h, along with 81.4% and 27.5% greater sizes compared to the Control and FLM group, respectively ($P<0.05$). FLM and FLM 150 were found to induce an earlier and more pronounced increase in CM particle size. This effect may be attributed to polyphenolics down-

regulating CM production in intestinal Caco-2 cells, thereby promoting further particle enlargement [25-26].

To identify the material basis of flaxseed lignans, we compared the effects of SDG and SECO (FLM metabolites) on CMs' particle size distribution after emulsion gavage. The SDG-supplemented emulsion delayed peak CMs' size occurrence to 4–6 h (371 nm), exhibiting 20.7% and 35.8% reductions compared to FLM- and FLM 150-containing emulsions at equivalent timepoints (both $P<0.05$), followed by gradual reduction to baseline by 12–24 h. Similarly, SECO supplementation postponed maximal CMs size to 2–4 h (454.32 nm), showing 11.1% decrease versus FLM 150 emulsion ($P<0.05$). Both SDG and SECO groups ultimately restored CMs sizes to initial levels at 12–24 h, contrasting with sustained CMs enlargement in FLM and FLM 150 groups. Interesting, these differential kinetics suggested that the CM synthesis-enhancing effects and lipid transport potentiation observed in FLM and FLM150 groups primarily stem from their inherent oligomeric structures rather than monomeric SDG/SECO derivatives. The mechanism of its action still requires further investigation.

The effects of FLM and FLM 150 on lipid oxidation levels of lymph after administered FO emulsions were presented in Figures 4a and 4b. Following FO administration, lymph LPO levels exhibited temporal fluctuations, starting at 0.4 μmol/L (0-1 h), peaking at 28.75 μmol/L (4-6 h), and then declining. Although the Control group showed significantly elevated initial levels (0-1 h), its peak value was 25% lower than that of the non-emulsified oil group ($P < 0.05$). FLM and FLM 150 supplementation achieved the maximum LPO reductions of 70.7% (FLM group) and 56.44% (FLM 150 group) compared to Control (both $P<0.05$), with SDG/SECO additives showing intermediate inhibitory effects. The highest malondialdehyde (MDA) levels in lymph of FO and Control group occurred at 1-2 h (30.4 nmol/L) and 2-4 h (28.5 nmol/L), respectively. Notably, Control group showed 42.3% lower MDA levels than FO at 4-6 h ($P<0.05$), indicating the suppressed lipid oxidation during digestion by nanoemulsification. Moreover, FLM further reduced MDA levels by 61-93% versus Control group ($P<0.05$), with FLM 150 exhibiting maximum inhibition (93% reduction compared to FO group). We therefore concluded that thermal-

processed FLM150 specifically delayed secondary oxidation of lipid. This was evidenced by a 45-68% reduction in volatile aldehyde derivatives compared to the Control group[27].

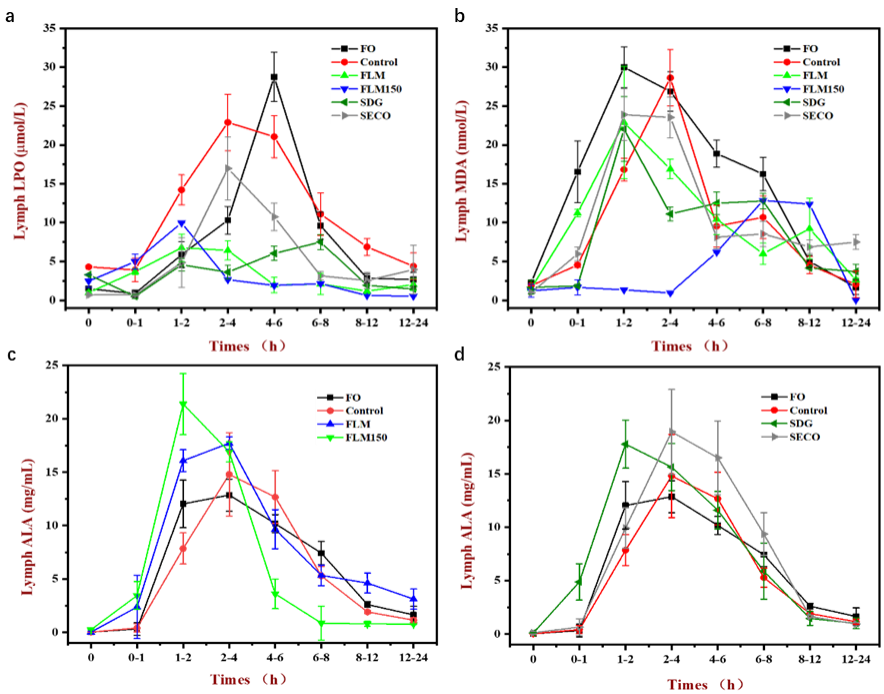

Fig.4 Effect of FLM, FLM150-enriched emulsion on lymphatic lipid oxidation (a,b) and ALA absorption (c,d) in rats after gavage.

Figures 4c and 4d illustrated the effects of FLM and FLM 150 on ALA absorption kinetics. Baseline lymphatic ALA concentrations showed no intergroup differences (0.03 mg/mL) across all six experimental groups. FO administration yielded the highest lymphatic ALA concentration of 12.85 mg/mL at 2-4 h, followed by gradual decline to 2.1 mg/mL by 8-24 h. The Control group achieved a 28.7% higher peak concentration (16.54 mg/mL at 2-4 h) and faster elimination (1.14 mg/mL at 12-24 h) than FO group, indicating nanoemulsification enhanced absorption efficiency of ALA. Besides, FLM further amplified absorption dynamics, reaching a maximum concentration of 20.90 mg/mL at 2-4 h, representing 66.7% increases over Control ($P<0.05$). Notably, the peak ALA concentration was advanced to 1-2 h by FLM 150, reaching levels that were 348%, 493%, and 72.2% higher than those in the FO group, Control group, and FLM group (0-1 h), respectively ($P < 0.05$). These accelerated absorption results also correlated with Caco-2 intestinal epithelium model findings. Therefore, combined in vivo and in vitro evidence confirmed that thermal

processing may convert FLM into another bioactivator. This conversion: 1) shifts ALA absorption kinetics from a sustained-release (FLM) to a rapid-onset (FLM-150) pattern via ester bond cleavage; 2) enhances ALA partitioning into lymph by improving micellar incorporation; and 3) maintains the structural stability of oligomeric flaxseed lignans, a domain critical for prolonging intestinal retention of ALA.

The effects of FLM and FLM 150 on fatty acid profiles in rat lymph were delineated Supplemental Figure 3. Lymphatic lipids in all groups predominantly comprised C16:0, C18:0, C18:1, C18:2, and C18:3 (collectively accounting for >95% of total content). The Control group exhibited 10.8% higher C18:3n-3 proportions than pure FO during 0–2 h ($P<0.05$), confirming enhanced ALA gastrointestinal lipolysis and lymphatic transport efficiency through nanoemulsification. Notably, FLM significantly elevated lymphatic C18:1 (oleic acid) and C18:2 (linoleic acid) levels by 18.2% and 14.6% versus Control group (both $P<0.05$), accompanied by increased metabolic derivatives including γ-linolenic acid (18:3n-6) and arachidonic acid (20:4n-6). The FLM-150 emulsion showed superior performance, achieving 22.4% higher C18:3n-3 levels than other formulations ($P<0.01$). This demonstrated FLM-mediated optimization of essential fatty acid bioavailability for subsequent metabolism. Besides, thermal processing likely enhanced FLM-150's amphiphilic properties through ester bond cleavage, facilitating mixed micelle incorporation and preferential lymphatic partitioning of n-3 fatty acids [20]. These structural modifications position FLM-150 as a dual-function excipient that simultaneously enhances lipid transport efficiency and preserves oxidative stability in emulsion-based delivery systems.

2.3 Lipidomics analysis the intracellular lipid resynthesis of absorbed ALA

Supplemental Fig. 2 presented the supervised partial least squares-discriminate analysis (PLS-DA) of lipid metabolism in lymph fluid from six rat groups. The permutation tests (100 iterations) demonstrated all p-values < 0.01 (Supplemental Fig. 2 h-i), confirming the model's predictability, high stability, and absence of overfitting[28]. As shown in Supplemental Figs. 2 a-f, distinct temporal clustering patterns were observed across experimental groups. Notably, significant differences emerged in lipid composition between rats administered FO and Control

group at various collection intervals. In the FO group, lymph samples exhibited an upward migration trajectory over time, with particularly pronounced differentiation between specimens collected at 4-6 h and 6-8 h compared to other intervals, indicative of peak lipid composition abundance during these periods[29]. The Control group displayed analogous temporal dynamics, though maximal lipid abundance manifested later in the 8-12 h and 12-24 h collection windows. These temporal shifts suggested differential lipid absorption kinetics between conventional FO and emulsions, potentially reflecting formulation-dependent variations in digestive processing and lymphatic transport efficiency[30].

Supplemental Fig. 1 displayed the results of multivariate analysis using variable importance in projection (VIP) scores to identify lipids with significant compositional differences across six experimental rat groups. The heatmap highlighted the top 15 lipid metabolites ranked by VIP values in rat lymph fluid, revealing formulation-specific and time-dependent variations. In rats administered FO, the most discriminative lipids included eight phosphatidylcholines (PCs), two oxidized phosphatidylethanolamines (PEs), two triglycerides (TGs), two diglycerides (DGs), and LPE 16:0. In contrast, the FO emulsion group exhibited nine TGs, five lysophosphatidylcholines (LPCs), and one PC as key differential lipids. Notably, distinct lipid profiles emerged in emulsion groups supplemented with bioactive compounds. The FLM group showed 13 TGs, one DG, and MG 18:0 as the dominant discriminative species. Similarly, the FLM150-supplemented emulsion group demonstrated six PCs, three phosphatidylinositols (PIs), and MG 18:0 with the highest VIP scores. The SDG group displayed a unique lipid signature comprising 12 TGs (including seven oxidized forms), one phosphatidylglycerol (PG), one PI, and one PC. Conversely, the SECO group featured 7 TGs, 6 FFAs, and 2 PCs as the most significant discriminative lipids. These results demonstrated that co-administration of FO emulsions with FLM, FLM150, SDG, or SECO modulated both the temporal sequence and structural configuration of lipid resynthesis in small intestinal epithelial cells. Compared to FO, emulsification with S90 and the incorporation of FLM or SDG into the emulsion enhanced TG synthesis, whereas FLM150 supplementation preferentially promoted PC synthesis. Intriguingly, SECO introduction exhibited an inhibitory

effect on TG resynthesis, suggesting the specific regulatory roles in lipid metabolism of different flaxseed lignan.

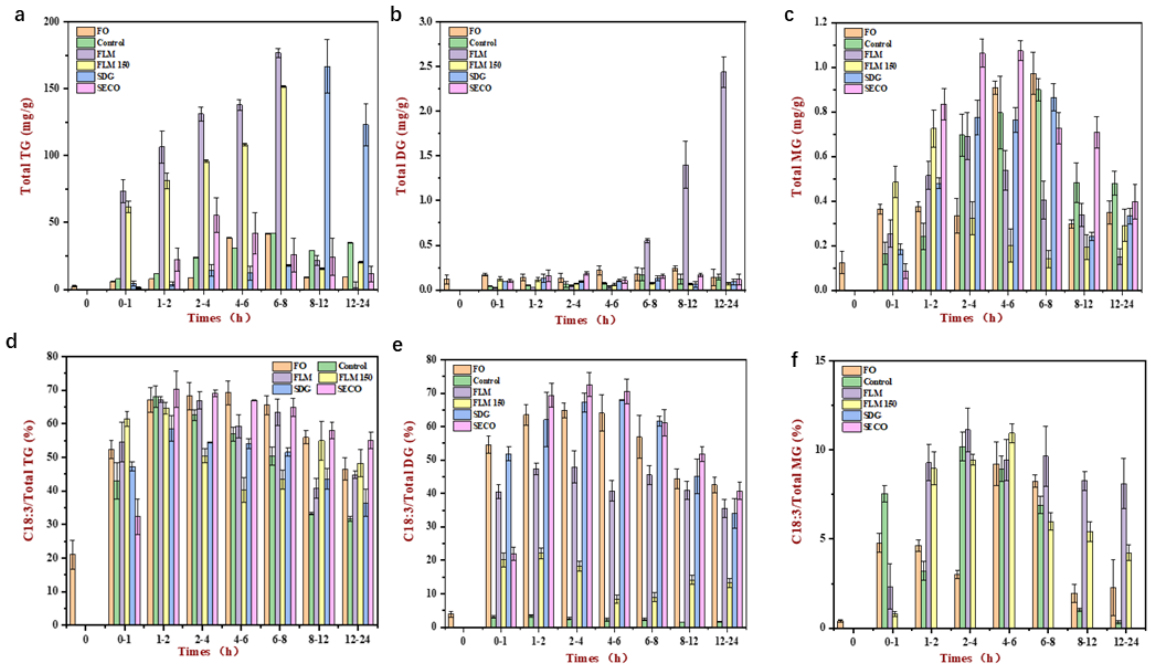

Fig.5

The lipid types (a,b,c) and the proportion (d,e,f) of C18:3 in lymph with 24h after gavage using flaxseed oil and FLM, FLM 150, SDG or SECO enriched flaxseed oil emulsions

To validate these findings, quantitative comparative analysis of lymphatic lipid profiles was conducted. Figure 5 illustrated the temporal dynamics of TGs, DGs, and MGs resynthesis in intestinal epithelial cells following administration of distinct emulsion formulations. Figure 5a revealed that baseline TG concentration in pre-gavage lymph fluid was 0.34 mg/g. Compared to Control group, FLM or FLM150 group exhibited significantly elevated TG concentrations during 0–8 h, peaking at 6–8 h (176.64 ± 3.34 mg/g, 3.21-fold higher, $p < 0.05$). In contrast, SDG group displayed delayed TG accumulation, with maximal concentrations (166.64 ± 6.64 mg/g, 4.71-fold higher, $p < 0.05$) persisting through 12–24 h. SECO group showed transient TG elevation, reaching a peak of 54.36 ± 6.64 mg/g (2.14-fold higher, $p < 0.05$) at 2–4 h before declining, indicative of suppressed TG resynthesis. DG concentrations exhibited a baseline of 0.14 mg/g (Figure 5b). FLM group demonstrated a marked increase in DG levels during 6–24 h, peaking at 12–24 h (2.44 ± 0.17 mg/g), whereas FLM150, SDG, and SECO groups showed no significant changes with Control group. MG dynamics revealed a baseline of 0.11 mg/g(Figure 5c). Both the Control and

FO groups reached the highest MG concentration (0.97 ± 0.09 mg/g) at 6–8 h, while FLM and FLM150 groups peaked earlier (1–2 h, 0.72 ± 0.08 mg/g). SECO group displayed MG accumulation at 2–6 h (1.07 ± 0.04 mg/g), followed by a decline.

ALA (C18:3 n-3) incorporation into lipid species exhibited formulation-dependent patterns. For TGs, the Control group showed biphasic ALA enrichment, peaking at 66.34% during 1–2 h (Figure 5d). The FLM150 group demonstrated a 41.8% increase in ALA proportion within 0–2 h ($p < 0.05$ vs. controls), followed by a marked decline. Notably, FLM, SDG, and SECO exerted no significant effects on ALA incorporation into TGs, suggesting their regulatory mechanisms might be independent of ALA metabolic pathways. For DGs, the FLM group maintained a stable ALA proportion of 42.5%, significantly higher than other groups (Figure 5e). The FLM150 group reached a maximum ALA proportion of 20% before declining, while unmodified FO maintained 53–62% ALA in DGs, with no differences observed in SDG or SECO groups. For MGs, the FLM group exhibited sustained high ALA incorporation (10.6% at 2–4 h), whereas the FLM150 group peaked at 10.6% (4–6 h) before reverting to baseline (Figure 5f). No ALA was detected in MG fractions of SDG or SECO groups. These findings indicated that FLM enhances DG resynthesis from lipolytic products in enterocytes, while FLM150, SDG, and SECO show negligible effects on this process.

Figure 6 delineated phospholipid resynthesis patterns post-gavage. Figure 6a demonstrated a baseline PCs concentration of 1.23 mg/g. The SECO group exhibited a dramatic PC surge during 0–8 h, peaking at 6–8 h (76.04 ± 2.72 mg/g, 16.44-fold vs. controls, $p < 0.05$), whereas FLM, FLM150, and SDG groups showed reduced PC levels from 4–24 h. Lysophosphatidylethanolamine (LPE) and PEs levels displayed baselines of 8.25 μg/g and 125 μg/g, respectively. FLM, FLM150, and SDG groups showed about 66% reduction in LPE content compared to controls, while the SECO group reached maximal LPE levels at 12–24 h (22.56 ± 2.54 μg/g). PE concentrations surged in FLM and FLM150 groups during 0–2 h (650–700 μg/g), with sustained 50–500% elevation than Control during 8–24 h. It was indicated that ALA incorporation into phospholipids revealed distinct regulatory effects by different flaxseed lignans.

For PCs, the SECO group maintained the highest ALA proportion (28%) throughout 1–24 h, whereas FLM, SDG showed a reduced ALA proportion. It indicated that SDG and SECO enhanced ALA incorporation into LPE and PE. Moreover, SECO achieved an increase of ALA incorporation into proportions LPE and PE (28% and 9.6% respectively), indicating its unique capacity to promote ALA-driven phospholipid synthesis.

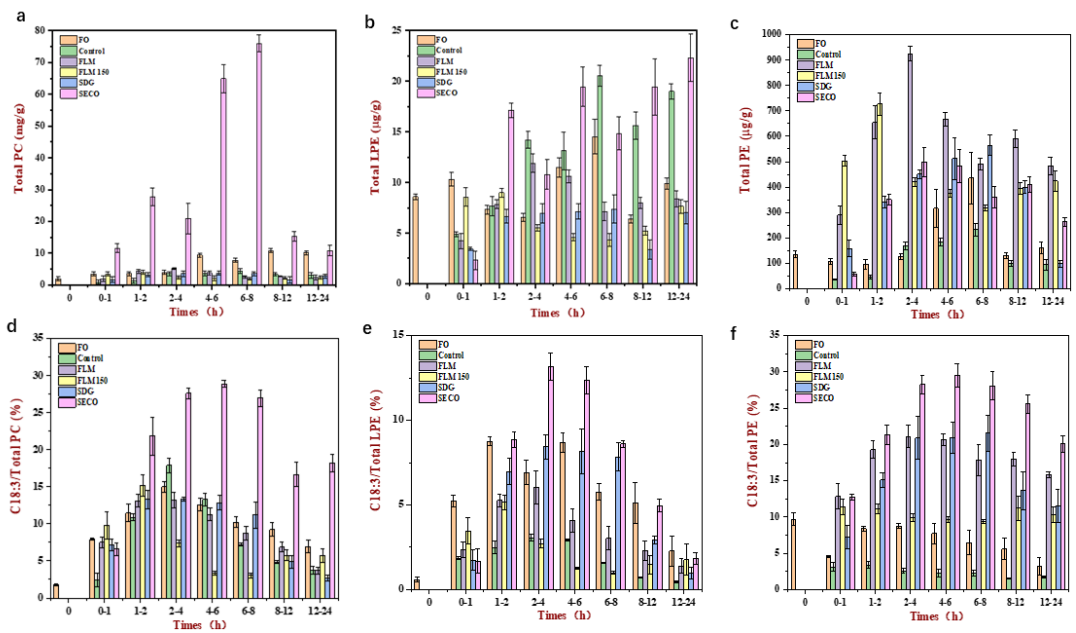

Fig.6 The phospholipid types (a,b,c) and the proportion (d,e,f) of C18:3 in lymph with 24h after gavage using flaxseed oil and FLM, FLM 150, SDG or SECO enriched flaxseed oil emulsions

These findings collectively demonstrated that FLM synergizes with FO emulsions to amplify DG resynthesis, whereas SECO uniquely enhances PC synthesis and ALA integration into phospholipids. The temporal shifts in lipid resynthetic dynamics reflected flaxseed lignan-dependent modulation of lipid synthesis enzyme kinetics and lipid transport efficiency[31]. Notably, SECO selectively enhanced ALA incorporation into phospholipids independently of its effects on neutral lipid metabolism. Therefore, as summarized in Figure 7, the mechanistic impact of FLM and its processed derivatives on enterocytic lipid resynthesis involves distinct pathways. Co-administration of FLM or FLM150 with FO emulsions reduced lymphatic MGs levels while elevating TG concentrations compared to the standard emulsion group. This suggested that FLM

and FLM150 promote the re-esterification of MG into TG. FLM exhibited additional enhancement of DG synthesis, outperforming FLM150 in this regard. We hypothesized that FLM concurrently upregulates both monoglyceride acyltransferase (MGAT) and diglyceride acyltransferase (DGAT) activities, whereas FLM150 may selectively enhance DGAT activity, thereby driving TG accumulation in lymph[32]. In phospholipid metabolism, FLM, FLM150, and SDG reduced lymphatic LPE levels compared to controls, implying their potential to stimulate lysophospholipid acyltransferase activity and accelerate PE synthesis. In contrast, SECO had no effect on LPE-to-PE conversion but markedly elevated PC levels. The differential redistribution of ALA across lymphatic lipid species, particularly its SECO-driven enrichment in phospholipids, may critically influence its systemic metabolic fate and bioavailability [28(23)]. These observations underscored the importance of emulsion formulation and flaxseed lignans in modulating lipid metabolic trajectories, offering targeted strategies to optimize lipid-soluble nutrient delivery or mitigate metabolic imbalances.

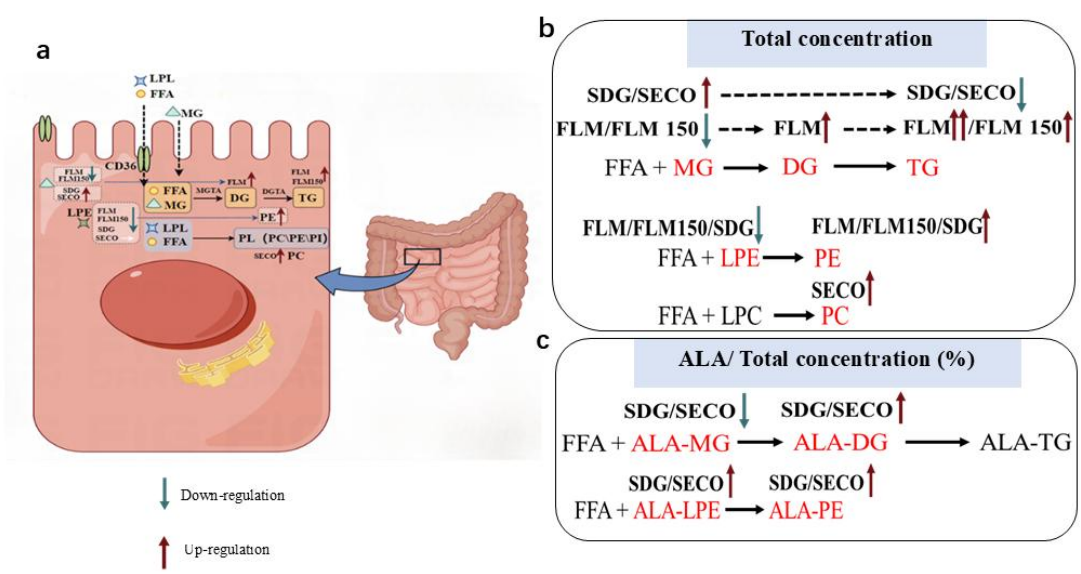

Fig.7 a: Schematic diagram of LPL, FFA and MG absorption by intestinal epithelial cells and intracellular lipid metabolism; b: Regulatory pathway of FLM, FLM150, SDG, and SECO on lipid metabolism within intestinal epithelial cells; c: Regulatory of FLM, FLM150, SDG, and SECO on ALA involvement in different lipid metabolic pathways within intestinal epithelial cells. (It reflected that the mechanistic impact of FLM and its processed derivatives on enterocytic lipid resynthesis involves distinct pathways. In the pathway of TG synthesis from FFA and MG, co-administration of FLM or FLM150 with FO emulsions reduced lymphatic MG levels while elevating TG concentrations compared to the standard emulsion group (FO emulsion without

FLMs). FLM exhibited additional enhancement of DG synthesis, and outperforming FLM150 in this regard. In phospholipid metabolism (from LPE to PE and PC), FLM, FLM150, and SDG reduced lymphatic LPE levels compared to controls, implying their potential to stimulate lysophospholipid acyltransferase activity and accelerate PE synthesis. In contrast, SECO had no effect on LPE-to-PE conversion but markedly elevated PC levels. Regarding the lipid metabolic process involving ALA (Figure c), the co-intake of SDG or SECO with FO, respectively, could enhance the metabolic flux of ALA toward DG and PE. The differential redistribution of ALA across lymphatic lipid species, particularly its SECO-driven enrichment in phospholipids, may critically influence its systemic metabolic fate and bioavailability.)

In our study, FLM 150 was identified as a promising effect on improving the bioavailability of ALA in emulsion system by the regulation of ALA micellar absorption and in vivo transport. Based on those novel results, the regulatory mechanisms of FLM and FLM 150 on ALA absorption was systematically investigated. Key findings revealed that the interactions between FLM 150 and mucin proteins in the intestinal lumen significantly increased mucus layer apparent viscosity, thereby inhibiting ALA-loaded micelle penetration through the mucus layer. Then, Caco-2 cell transport assays demonstrated that FLM 150 and SDG supplementation emulsions markedly enhanced ALA absorption by 95% compared to the FO emulsion, indicating the improved epithelial uptake efficiency by flaxseed lignans. Notably, FLM 150-enriched emulsion exhibited a 493% increase ($P < 0.05$) in lymphatic ALA concentration within 0–1 h compared to the control emulsion, indicating its rapid absorption-enhancing effects. Finally, lymphatic lipidomic profiling from the rat cannulation model further revealed formulation-dependent metabolic outcomes: SECO co-administered with FO emulsion promoted PC synthesis by lysophosphatidylcholine remodeling, while FLM, FLM 150, or SDG supplementation preferentially enhanced TG resynthesis. The above results demonstrated the enhanced absorption effects of ALA by FLM and its heat treatment products FLM150, and their differential regulation on lipid metabolism in small intestinal epithelial cells. Therefore, the results hold significant implications for achieving efficient ALA intake, optimizing dietary structure balance. However, it also suggested the potential application of flaxseed lignans on modulating the subsequent metabolism and biological activity of ALA in vivo. But it needs to a further investigation to provide a theoretical foundation for the development of flaxseed lignans and FO in functional foods.

3. Methods

3.1 Chemicals and reagents

FO was originated from Hongjingyuan Oil Co. Ltd (Xilingol, China), which ALA content is 50.4%. Sunflower lecithin sunlipon™ 90 (S90) was provided by a commercial supplier (Perimondo, New York, NY, USA). Secoisolariciresinol diglycoside (SDG, 97%), secoisolariciresinol (SECO, 95%), pancreatin, lipase (from porcine pancreas), as well as bile extract (porcine) were offered by Sigma-Aldrich (Saint Louis, MS, USA). Other reagents were purchased from Sinopharm Chemical Reagent Co., Ltd (Beijing, China).

3.2 FLM and its heat-treated products preparation

FLM was extracted according to our previous study[20]. In brief, flaxseed hull powder (FHP, 20 g) was defatted by incubating with 100 mL n-hexane at 25 ℃ for 24 hours. Defatted flaxseed hull powder (20 g) was subjected to three extractions using 100 mL of 70% ethanol-water (V/V) for 24 h. FLM extract was concentrated using rotary evaporators (IKARV10D, Germany) to about 50 mL, and further purified using a C18 solid-phase extraction column (Waters, C18, 5 cm). A C18 SPE cartridge was first conditioned with 5 mL of methanol to activate the hydrophobic C18 bonded phase, immediately followed by equilibration with 5 mL of ultrapure water to create a suitable environment for sample retention. A 3 mL aliquot of the sample was loaded, after which the column was washed with 5 mL of 50% (v/v) aqueous methanol. Elution was carried out with 5 mL of 80% (v/v) aqueous methanol to obtain the purified FLM.

The purified FLM was concentrated using a rotary evaporator (IKARV10D, Germany) and vacuum-freezing dryer and then stored at -18 ℃ for in-depth analysis. Following purification, the purity of FLM was estimated to be greater than 95% using the peak area normalization method. Heat-treated FLMs (FLM 150) were prepared by treating FLM in oil bath at 150 ℃ for 30 min to simulate baking process, which were concentrated by drying with a vacuum freezing dryer and then stored at -18 ℃ for in-depth analysis.

3.3 Preparation of flaxseed lignan-enriched FO emulsion

To evaluate the physiological effects of ALA in a natural complex food matrix, the FO with

high content ALA (50.4%) was used to prepare emulsion system. In details, FO emulsions were composited by 20% FO (w/w) and 80% (w/w) aqueous phase (3% S90 solutions). FLM or FLM-150 (0.5 mg/mL) were added in aqueous phase before emulsion preparation as experimental group, SDG or SECO were added in another S90 solutions respectively as positive control group. FO emulsions were prepared using a high-speed blender (IKA, T25, Germany) at 10000 rpm for 5 min following a microfluidizer (model M-110L, Microfluidics, Newton, MA) at 12,000 psi for four cycles.

3.4 In vitro absorption simulation of flaxseed lignan enriched FO emulsion

Oral, gastric and intestinal three-steps in vitro INFOGEST 2.0 gastrointestinal tract simulation method was used in this study with slight modification[33-34]. The mixed micelles of FO emulsions after intestinal digestion were used to simulate the process of ALA absorption.

Extraction of Intestinal Mucin. Small intestinal mucus was extracted from *ex vivo* porcine small intestine according to Feng et al.[13]. In detail, fresh porcine small intestine was obtained from healthy pig (Wuhan, China) and washed using deionized water three times. And then mucus extractions were carefully scraped from small intestine following centrifugation at 5000 rpm for 10 min. The lower layer was fresh small intestinal mucus, which was stored at -80℃ for further use.

Construction of reconstituted mucous layer. Frozen mucin was thawed at 37℃ and kept for 2h to ensure the recovery of gel structure. Mucin (150 μL) was loaded into a 12-well Transwell insert (0.4 μm pore size, Corning), which further labeled using Alexa Fluor-conjugated WGA and allowed to equilibrate for 60 min. Then, 0.5 mL of BODIBY 488-C12 labeled mixed micelle (obtained from 2.4.1) were loaded to the apical sides. The mucus gels were washed two times with phosphate-buffered saline after 10 min permeation and fixed with 75:25 ethanol/acetic acid (v/v) for 60 min. The Z-scans of a wide area of mucus gels were observed on a Leica Confocal Laser Scanning Microscope (Germany).

35 Mixed micelles of FO emulsions absorption by small intestinal epithelial cells

Caco-2 cells were cultured in DMEM containing 10%FBS, and 100 U/mL

penicillin/streptomycin/glutamine in T25 culture bottle, which was changed every other day until the cells were 80% ~ 90% confluent. The cells were kept at 37 C in a humidified atmosphere of 95% air and 5% CO_2, and Caco-2 cells only in passage 25~45 were used in this study[35].

For the experiments, cells were seeded in 12-well Transwell plates apical sides at 1×10^6 cells per well and grown under the same conditions as those described above. Basolateral sides were added 1.5 mL of DMEM. The experiments were performed at 21 days post seeding. Transepithelial electrical resistance (TEER) was measured during the construction of Caco-2 cells model. The TEER value of Caco-2 cultured in each transwell chamber was around 400 Ω/cm^2 indicating the formation of tight monolayers. TEER value was calculated according to Eq. (1).

$$TEER\ value = (R - R_0) \times A \quad (1)$$

Where R was the TEER value for transwell dish with Caco-2 cells growing, R_0 was the TEER value for transwell dish without Caco-2 cells (only had DMEM), A was the film area.

Mixed micelles obtained in 2.4.1 was used to evaluate the absorption of FFAs. Briefly, a cytotoxicity test was designed first. The apical sides of Transwell were added 0.5 mL mixed micelles (diluted 50 times using DMEM), Basolateral sides of Transwell were added 1.5 mL DMEM. the samples were obtained at 1, 30, 60, 90 and 120 min during the culture at 37℃ in cell incubator for 2 h.

3.6 Rat thoracic lymphatic duct cannulation experiment

Male Sprague-Dawley rats (300 ± 20 g) were housed for at least 3 days before the experiment in a controlled environment with constant temperature (25℃) and humidity with free water and food access. SD rats were fasted with free access to water 24 h before the surgery. Each rat was placed under slight isoflurane anesthesia (1 L oxygen flow containing 0.25% of isoflurane solution) and a polyethylene catheter was inserted into the main mesenteric lymph duct.

At least 6 rats were cannulated per group. Lymph collection experiments were performed after 3 mL intragastric gavage emulsions. Besides, un-emulsified FO (0.6 mL FO and 2.4 mL water) was set as positive control. Saline supplementation (5 mL, 0.9% NaCl) was delivered intraperitoneally at 4 h and 12 h post-dosing. And Lymph was collected in pre-chilled EDTA tubes

during intervals of 0–1 h, 1–2 h, 2–4 h, 4–6 h, 6–8 h, 8–12 h, and 12–24 h, with a 1 mL pre-dose baseline sample stored at −80°C.

Rats were euthanized via carbon dioxide (CO_2) asphyxiation. Animals were individually placed in a sealed induction chamber. CO_2 was introduced gradually at a displacement rate of 30-50% of the chamber volume per minute to minimize distress. Subjects remained in the chamber until at least one minute after the cessation of breathing. Death was verified by absence of corneal reflex and confirmed by a secondary physical method (cervical dislocation or bilateral thoracotomy). All experiments conformed to the Guidelines for the Handling and Training of Laboratory Animals.

3.7 The particle size and morphology characteristics of lymph chylomicron (CMs)

The sizes and morphology characteristics of the lymph CMs were measured in each diet group throughout the kinetics of lipid absorption using a static light scattering instrument (Mastersizer 3000, Malvern Instruments, Westborough, MA). The morphology characteristics of lymph CMs was captured by cryo-scanning (Cryo-SEM, SU8010, Hitachi, Tokyo, Japan). Briefly, lymph CMs (5.0–10.0 μL) was transferred into a cryo-preparation chamber after frozen in liquid nitrogen, then cut into the cross-section at −90 °C and 1.3×10^{-6} mbar, sputter-coated at 10 mA for 30 s. The samples were observed using a Cryo-SEM at 3 kV.

3.8 ALA absorption kinetics

The fatty acid composition of *chylomicron* in collected lymph was detected according to the methods in our lab.[36], 150 μL of lymph was mixed with 20 μL of the internal standard (methyl ester of 17-carbon fatty acid, 5.00 mg/mL) and 2 mL of 5% concentrated sulfuric acid/methanol solution, 300 μL of toluene in 15 mL gland bottle. Then, gland bottles were sealed using an aluminum cap with a polytetrafluoroethylene pad. After incubating at 95 ℃ for 1.5 h (water bath), 2 mL of 0.9% NaCl solution were added in cooled gland bottle. Finally, 1 mL of n-hexane were added to extracts, the mixture was centrifuged at 10000 × g for 5 min. The supernatant obtained to detected using gas chromatograph (GC), which equipes FID hydrogen flame ionization detector, FastFAME column(30 m × 0.25 mm, 0.25 μm). The inlet temperature and detector temperature

were set as 250℃ and 260℃ respectively, the shitter ratio was 20:1. The chromatographic column initial temperature was 80 ℃ and maintained 0.5 min. Then, the chromatographic column temperature was raised to 165℃ at 40 ℃/min and maintained 1 min. Immediately after that, the chromatographic column temperature was raised to 230 ℃ at 4℃/min and maintained at this temperature for 6 min. The ALA concentration in lymph chylomicrons according to Eq.2:

$$\text{ALA concentration (mg/mL)} = \frac{S1}{S2} \times \frac{N}{M} \quad (2)$$

Where S1 is the peak area of ALA, S2 is the peak area of internal standard, N is the volume of added internal standard (20 μL), M is the weight of samples.

3.9 Total lipid extraction and Lipidomics analysis using UPLC-QTOF-MS/MS

Total lipid extraction and Lipidomics were analyzed according to the methods in our lab. Aliquot 150 μL of the lymphatic fluid were put in disposable test tubes, another 2 mL of chromatography-grade methanol added, and the mixture incubated at -20°C overnight to precipitate proteins. After overnight incubation, aliquot 2 mL of dichloromethane and 20 μL of internal standard were added to the mixture and vortexed the mixture for 1 hour. Besides, 2 mL of dichloromethane and 1.6 mL of ultrapure water were added and vortexed for 30 minutes, following centrifuged at 5000 rpm for 10 minutes and collect the lower-phase solution (first lipid extract). Then, another 4 mL of dichloromethane were added to the remaining samples and vortexed for 10 minutes, following centrifuged at 5000 rpm for 10 minutes to collect the lower-phase solutions. Finally, the lower-phase solutions from all three extractions were combined, evaporated the pooled solution to dryness under a nitrogen stream. The dried residue was reconstituted using 100 μL of methanol:dichloromethane (1:1, v/v) and detected using HPLC (LC-20, Shimadzu, Tokyo, Japan) coupled Triple TOF 5600 system (ABSciex, USA) with ESI source under positive and negative modes.

The instrument sample tray and autosampler temperature were set at 4°C, the column temperature was maintained at 60°C, with a flow rate of 0.4 mL/min. The injection volumes for the positive ion mode and negative ion mode were 2 μL and 6 μL, respectively. Full fat internal standards include 1,3-dipentadecanoyl-2-oleyol (d7)-glycerol (d7-TAG-15:0/18:1/15:0), 1-

pentadecanoyl-2-oleyol (d7)-sn-glycerol (d7-DAG-15:0/18:1), 1-pentadecanoyl-2-oleoyl (d7)-sn-gly-cero-3-phosphocholine (d7-PC-15:0/18:1), 1-pentadecanoyl-2-oleoyl (d7)-sn-glycero-3-phosphoethanolamine (d7-PE-15:0/18:1), 1-pentade-canoyl-2-oleoyl (d7)-sn-glycero-3-phospho-L-serine (d7-PS-15:0/18:1), 1-pentadecanoyl-2-oleoyl (d7)-sn-glycero-3-phosphoino-sitol (d7-PI-15:0/18:1), 1-pentadecanoyl-2-oleoyl (d7)-sn-glycero-3-phosphate (d7-PA-15:0/18:1), 1-penta-decanoyl-2-oleoyl (d7)-sn-glycero-3-phospho-rac-(1 ' -glyce-rol) (d7-PG-15:0/18:1), N-pentadecanoyl-D-erythro-sphingosine (Cer-d18:1-d7/15:0), Palmitic acid (d4-C16:0), fatty acid methyl ester (FAME37) standard, methyl heptadecanoate (C17:0) and N-Oleoyl-D-erythro-sphingosylphosphorylcholine (SM-d18:1/18:1-d9).

The mobile phases A and B were H_2O/MeOH/CAN (1:1:1, v/v, 5mM NH_4AC) and IPA/CAN (1:1:1, v/v, 5 mM NH_4AC), respectively. Chromatographic separation was achieved with an Agilent Phenomenex Kinetex (100 mm×2.1mm, 2.6μm, Agilent Ltd., USA), at a flow rate of 0.3 mL/min using the following gradient: 0~0.5 min 20%B, 0.5-1.5 min 20~40%B, 1.5~3.0 min 40~60%B, 3.0~13.0 min 60~98%B, 13.0~13.1 min 98~20%B, 13.1~17.0 min, 20%B. The acquired mass range was set as 100-1200 Da for TOF and product ion scans respectively. The ESI source parameters were: nebulizer and heater gases set at 55 psi, curtain gas at 30 psi, and heater temperature at 600 °C. The ion spray voltage was 5 500 and -4 500 V for ESI+ and ESI- modes, respectively. The declustering voltage (DP) were set at 80V (+) and -80V (-) and collision energy (CE) were set at 10V (+) and -30V (-). The nebulizer gas (GS1) and heater auxiliary gas (GS2) were both maintained at 50 ps with the curtain gas (CUR) at 35 psi. The ion source temperature was 600°C, using nitrogen as both the nebulizing gas and auxiliary gas.

Took equal samples to prepare quality control (QC) samples. QC samples were injected every 10 samples throughout the analytical batch to assess the stability of the instrument.

3.10 Statistical analysis

All assays were performed in triplicate, and the data are expressed as mean ± SD (n=3). One-Way ANOVA was performed to analyze the significant differences between data ($p < 0.05$) using SPSS 24 (SPSS Inc., Chicago, IL, USA). The data of UPLC-Qtof-MS/MS were analyzed using

MSDAIL and Peakview 2.0 software. Global lipidomic principal component analysis (PCA), heatmap, and correlation analysis were performed using software of MetaboAnalyst 4.0.

Knowledgments

The authors gratefully acknowledge the financial support from National Natural Science Foundation of China (32402168 and 32072267), Research Funding of Wuhan Polytechnic University NO.2025R2050, and China Agriculture Research System of CRAS-14. We extend our gratitude to WETRYBIO Biotechnology (Shanghai) Co., Ltd. for providing rat thoracic lymphatic duct cannulation experimental technique and platform (WTPZ20221212001).

Data Availability Statement

The lipidomics were analyzed using Public Database MSDAIL and Peakview 2.0 software. Global lipidomic principal component analysis (PCA), heatmap, and correlation analysis were performed using software of MetaboAnalyst 4.0.

Competing Interests

I declare that the authors have no competing interests as defined by Nature Portfolio, or other interests that might be perceived to influence the results and/or discussion reported in this paper.

Author Contributions

Chen Cheng was responsible for the writing of original draft, methodology, and visualization. Xiao Yu was responsible for the writing of original draft and visualization. Lei Wang was responsible for the conceptualization and data analysis. Shuyi Li was responsible for conceptualization and formal analysis. Xu Chen was responsible for conceptualization, writing of original draft, and visualization. Qianchun Deng was responsible for supervision, conceptualization, and funding acquisition. Zhenzhou Zhu was responsible for conceptualization and visualization. All authors reviewed the manuscript.

References

1. Lai, H. T.; De, O. O., Marcia C; Lemaitre, R. N.; Mcknight, B.; Song, X.; King, I. B.; Chaves, P. H.; Odden, M. C.; Newman, A. B.; Siscovick, D. S., Serial circulating omega 3 polyunsaturated fatty acids and healthy ageing among older adults in the Cardiovascular Health Study: prospective cohort study. *BMJ* **2018,** *363*. DOI:10.1136/bmj.k4067
2. Lister, N. B.; Baur, L. A.; Felix, J. F.; Hill, A. J.; Marcus, C.; Reinehr, T.; Summerbell, C.; Wabitsch, M., Child

and adolescent obesity. *Nature Reviews Disease Primers* **2023,** *9* (1). https://doi.org/10.1038/s41572-023-00440-7

3. Barceló-Coblijn, G.; Murphy, E. J., Alpha-linolenic acid and its conversion to longer chain n-3 fatty acids: benefits for human health and a role in maintaining tissue n-3 fatty acid levels. *Progres*s in Lipid Research 2009, 48 (6), 355-374. https://doi.org/10.1016/j.plipres.2009.07.002
4. D'Aquila, T; Hung, Y.H.;Carreiro, A.; Buhman, K. K.; Recent discoveries on absorption of dietary fat: Presence, synthesis, and metabolism of cytoplasmic lipid droplets within enterocytes. *Biochimica et Biophysica Acta (BBA) - Molecular and Cell Biology of Lipids* **2016**, 1861(8),730-747. https://doi.org/10.1016/j.bbalip.2016.04.012
5. Damianos, J.; Abdelnaem, N.; Camilleri, M., Gut Goo: Physiology, Diet, and Therapy of Intestinal Mucus and Biofilms in Gastrointestinal Health and Disease. *Clinical Gastroenterology and Hepatology* **2025,** *23* (2), 205-215. https://doi.org/10.1016/j.cgh.2024.09.007
6. Murgia, X.; Pawelzyk, P.; Schaefer, U. F.; Wagner, C.; Willenbacher, N.; Lehr, C. M., Size-Limited Penetration of Nanoparticles into Porcine Respiratory Mucus after Aerosol Deposition. *Biomacromolecules* **2016**, 17(4), 1536-1542. https://doi.org/10.1021/acs.biomac.6b00164
7. Bao, C.; Liu, B.; Li, B.; Chai, J.; Li, Y., Enhanced Transport of Shape and Rigidity-Tuned α-Lactalbumin Nanotubes across Intestinal Mucus and Cellular Barriers. *Nano Letters* **2020,** 20.1352-1361. https://doi.org/10.1021/acs.nanolett.9b04841
8. Wang, D.; Jiang, Q.; Dong, Z.; Meng, T.; Hu, F.; Wang, J.; Yuan, H., Nanocarriers transport across the gastrointestinal barriers: The contribution to oral bioavailability via blood circulation and lymphatic pathway. *Advanced Drug Delivery Reviews* **2023,** *203*, 115130. https://doi.org/10.1016/j.addr.2023.115130
9. Cheng, C.; Yu, X.; Huang, F.; Peng, D.; Deng, Q., Effect of Different Structural Flaxseed Lignans on the Stability of Flaxseed Oil-in-water Emulsion: An Interfacial Perspective. *Food Chemistry* **2021**, 357, 129522. https://doi.org/10.1016/j.foodchem.2021.129522
10. Sugasini, D.; Devaraj, V. C.; Ramesh, M.; Lokesh, B. R., Lymphatic Transport of α-Linolenic Acid and Its Conversion to Long Chain n-3 Fatty Acids in Rats Fed Microemulsions of Linseed Oil. *Lipids* **2013**, 49(3), 225-233. https://doi.org/10.1007/s11745-013-3873-4
11. Feng, N.; Hu, J.; Liang, S.; Yang, X.; Zhu, X.; Feng, Y.; Zhao, X.; Tang, F.; Yang, J.; Wu, Q., Physical and oxidative stability of flaxseed oil-in-water emulsions prepared by natural lignin-carbohydrate complex. *International Journal of Biological Macromolecules* **2024,** *270*, 132154. https://doi.org/10.1016/j.ijbiomac.2024.132154
12. Wang, X.; Chen, H.; Xu, Y.; Deng, Q., The role of micro-structures in the aqueous phase of emulsion in lipid oxidation process. *Food Chemistry* **2025,** 464, *141760*. https://doi.org/10.1016/j.foodchem.2024.141760
13. Feng, G.; Han, K.; Yang, Q.; Feng, W.; Guo, J.; Wang, J.; Yang, X., Interaction of Pyrogallol-Containing Polyphenols with Mucin Reinforces Intestinal Mucus Barrier Properties. *Journal of Agricultural and Food Chemistry* **2022,** *70* (30), 9536-9546. https://doi.org/10.1021/acs.jafc.2c03564
14. Adolphe, J. L.; Whiting; S. J.; Juurlink, B. H. J.; Thorpe, L. U.; Alcorn, J., Health effects with consumption of the flax lignan secoisolariciresinol diglucoside. *British Journal of Nutrition* **2010,** *103* (7), 929-938. https://doi.org/10.1017/s0007114509992753
15. Habtemariam, S., The what and who of dietary lignans in human health: Special focus on prooxidant and antioxidant effects. *Trends in Food Science & Technology* **2020,** *106*, 382-390. https://doi.org/10.1016/j.tifs.2020.10.015

16. Wang, L.; Cheng, C.; Yu, X.; Guo, L.; Wan, X.; Xu, J.; Xiang, X.; Yang, J.; Kang, J.; Deng, Q., Conversion of α-linolenic acid into n-3 long-chain polyunsaturated fatty acids: bioavailability and dietary regulation. *Critical Reviews in Food Science and Nutrition* **2024**, 1-33. https://doi.org/ 10.1080/10408398.2024.2442064
17. Adlercreutz; Herman, Lignans and human health. *Critical Reviews in Clinical Laboratory Sciences* **2008,** *44* (5), 483-525. https://doi.org/10.1080/10408360701612942
18. Yang, X.; Guo, Y.; Tse, T. J.; Purdy, S. K.; Reaney, M. J. T., Oral Pharmacokinetics of Enriched Secoisolariciresinol Diglucoside and Its Polymer in Rats. *Journal of Natural Products* **2021**, 84 (6), 1816-1822. https://doi.org/10.1021/acs.jnatprod.1c00335
19. Cheng, C.; Wang, L.; Yu, X.; Huang, F.; Deng, Q., Structural identification and antioxidative activity evaluation of flaxseed lignan macromolecules: structure-activity correlation. *Food Science and Human Wellness* **2024,** *13* (6), 3224-3235. https://doi.org/10.26599/FSHW.2023.9250009
20. Cheng, C.; Yu, X.; Huang, F.; Wang, L.; Deng, Q., et al., Effect of heat-treated flaxseed lignan macromolecules on the interfacial properties and physicochemical stability of α-linolenic acid-enriched O/W emulsions. *Food & Function* **2024,** 15, 9524-9540. https://doi.org/ 10.1039/D4FO02663B21.
21. Abdulkarim, M.; Agulló, N.; Cattoz, B.; Griffiths, P.; Bernkop-Schnürch, A.; Borros, S. G.; Gumbleton, M., Nanoparticle diffusion within intestinal mucus: Three-dimensional response analysis dissecting the impact of particle surface charge, size and heterogeneity across polyelectrolyte, pegylated and viral particles. *European Journal of Pharmaceutics and Biopharmaceutics* **2015,** *97* , 230-238. https://doi.org/10.1016/j.ejpb.2015.01.023
22. Floor, E.; Su, J.; Chatterjee, M.; Kuipers, E. S.; Ijssennagger, N.; Heidari, F.; Giordano, L.; Wubbolts, R. W.; Mihăilă, S. M.; Stapels, D. A. C.; Vercoulen, Y.; Strijbis, K., Development of a Caco-2-based intestinal mucosal model to study intestinal barrier properties and bacteria–mucus interactions. *Gut Microbes* **2024,** *17* (1), 2434685. https://doi.org/10.1080/19490976.2024.2434685
23. Wilson, F. A.; Sallee, V. L.; Dietschy, J. M., Unstirred Water Layers in Intestine: Rate Determinant of Fatty Acid Absorption from Micellar Solutions. *Science* **1971,** *174* (4013), 1031-1033. https://doi.org/10.1126/science.174.4013.1031
24. Chloé, R.; Leslie, C.; Carole, K.; Laurence, F.; Charline, B.; Elisabeth, E. C.; Emmanuelle, M.; Emmanuelle, L.; Carole, V.; Marie-Caroline, M., Rapeseed Lecithin Increases Lymphatic Lipid Output and α-Linolenic Acid Bioavailability in Rats. *The Journal of Nutrition* **2020,** 150(11), 2900-2911. https://doi.org/10.1093/jn/nxaa244
25. Takechi, R.; Hiramatsu, N.; Mamo, J. C. L.; Pal, S., Red wine polyphenolics suppress the secretion and the synthesis of Apo B48 from human intestinal Caco-2 cells. *BioFactors* **2004**, 22(1-4):181-183. https://doi.org/10.1002/biof.5520220137
26. Pang, J.; Raka, F.; Heirali, A. A.; Shao, W.; Liu, D.; Gu, J.; Feng, J. N.; Mineo, C.; Shaul, P. W.; Qian, X.; Coburn, B.; Adeli, K.; Ling, W.; Jin, T., Resveratrol intervention attenuates chylomicron secretion via repressing intestinal FXR-induced expression of scavenger receptor SR-B1. *Nature Communications* **2023,** *14* (1), 2656. https://doi.org/10.1038/s41467-023-38259-1
27. Gobert, M.; Rémond, D.; Loonis, M.; Buffière, C.; Santé-Lhoutellier, V.; Dufour, C., Fruits, vegetables and their polyphenols protect dietary lipids from oxidation during gastric digestion. *Food & Function* **2014,** *5* (9), 2166-2174. https://doi.org/10.1039/c4fo00269e
28. Jia, W.; Wu, X.; Zhang, R.; Wang, X.; Shi, L., Novel insight into the resilient drivers of bioaccumulation perchlorate on lipid nutrients alterations in goat milk by spatial multi-omics. *Lwt* **2022,** *165,* 113717. https://doi.org/10.1016/j.lwt.2022.113717

29. Zhou, Z.; Zhang, Y. Y.; Xin, R.; Huang, X. H.; Li, Y. L.; Dong, X.; Zhou, D.; Zhu, B.; Qin, L., Metal Ion-Mediated Pro-oxidative Reactions of Different Lipid Molecules: Revealed by Nontargeted Lipidomic Approaches. *Journal of Agricultural and Food Chemistry* **2022,** *70* (33), 10284-10295. https://doi.org/10.1021/acs.jafc.2c02402
30. Trevaskis, N. L., The Mesenteric Lymph Duct Cannulated Rat Model: Application to the Assessment of Intestinal Lymphatic Drug Transport. *Journal of Visualized Experiments* **2015,** *97* (97), 52389. https://doi.org/10.3791/52389-v
31. Zhang, P.; Csaki, L. S.; Ronquillo, E.; Baufeld, L. J.; Lin, J. Y.; Gutierrez, A.; Dwyer, J. R.; Brindley, D. N.; Fong, L. G.; Tontonoz, P., Lipin 2/3 phosphatidic acid phosphatases maintain phospholipid homeostasis to regulate chylomicron synthesis. *The Journal of Clinical Investigation* **2019,** *129* (1), 281-295. https://doi.org/10.1172/JCI122595
32. Zembroski, A. S.; Xiao, C.; Buhman, K. K., The Roles of Cytoplasmic Lipid Droplets in Modulating Intestinal Uptake of Dietary Fat. *Annual Review of Nutrition* **2021,** *41* (1), 79-104. https://doi.org/10.1146/annurev-nutr-110320-013657
33. Brodkorb, A.; Egger, L.; Alminger, M.; Alvito, P.; Assunção, R.; Ballance, S.; Bohn, T.; Bourlieu-Lacanal, C.; Boutrou, R.; Carrière, F.; Clemente, A.; Corredig, M.; Dupont, D.; Dufour, C.; Edwards, C.; Golding, M.; Karakaya, S.; Kirkhus, B.; Le Feunteun, S.; Lesmes, U.; Macierzanka, A.; Mackie, A. R.; Martins, C.; Marze, S.; McClements, D. J.; Ménard, O.; Minekus, M.; Portmann, R.; Santos, C. N.; Souchon, I.; Singh, R. P.; Vegarud, G. E.; Wickham, M. S. J.; Weitschies, W.; Recio, I., INFOGEST static in vitro simulation of gastrointestinal food digestion. *Nature Protocols* **2019,** *14* (4), 991-1014. https://doi.org/10.1038/s41596-018-0119-1
34. Tan, Y.; Zhang, Z.; Zhou, H.; Xiao, H.; McClements, D. J., Factors impacting lipid digestion and β-carotene bioaccessibility assessed by standardized gastrointestinal model (INFOGEST): oil droplet concentration. *Food & Function* **2020,** *11* (8), 7126-7137. https://doi.org/10.1039/d0fo01506g
35. Gong, S.; Zheng, J.; Zhang, J.; Wang, Y.; Xie, Z.; Wang, Y.; Han, J., Taxifolin ameliorates lipopolysaccharide-induced intestinal epithelial barrier dysfunction via attenuating NF-kappa B/MLCK pathway in a Caco-2 cell monolayer model. *Food Research International* **2022,** *158,* 111502. https://doi.org/10.1016/j.foodres.2022.111502
36. Wang, L.; Yu, X.; Cheng, C.; Xu, J.; Xiang, X.; Tang, X.; Deng, Q., Flax lignans regulate the conversion of α-linolenic acid into n-3 LCPUFAs in mice ingesting sunflower phospholipid-stabilized nanoemulsions. *Food Science and Human Wellness* **2024**. https://doi.org/10.26599/FSHW.2024.9250371